

Low-energy $N\phi$ scattering from a pole-enhanced triangle diagram

Mao-Jun Yan,^{1,*} Chun-Sheng An,^{1,†} and Cheng-Rong Deng^{1,‡}

¹*School of Physical Science and Technology, Southwest University, Chongqing 400715, China*

(Dated: January 13, 2026)

We investigate low-energy $N\phi$ scattering driven by a pole-enhanced triangle diagram, in which the two-kaon-exchange contribution is promoted by the near-threshold $\Lambda(1405)$ pole in the NK subsystem. Using an unphysical kaon mass motivated by lattice simulations, we evaluate the $N\phi$ scattering length and find that this mechanism generates an attractive interaction with a magnitude of -1.5 to -0.5 fm. Spin-dependent effects are not treated explicitly and are expected to provide subleading corrections in the near-threshold region. We further analyze the low-energy behavior of the triangle-diagram amplitude and show that the scattering length performs a characteristic power-law dependence on the parameter δ , defined as the mass difference between the $K\bar{K}$ threshold and the ϕ meson. This threshold-driven behavior differs from that associated with van der Waals-type forces or the long-range tail of two-pion exchange, highlighting the role of three-body dynamics encoded in the pole-enhanced triangle diagram in shaping the near-threshold $N\phi$ interaction.

I. INTRODUCTION

OZI-suppressed interactions mediated by multi-gluon exchange have long been discussed in strong interactions. In particular, such mechanisms were introduced to nucleon-heavy quarkonium scattering in terms of a QCD van der Waals-type interaction [1, 2], where an effective Yukawa potential, $V_{(Q\bar{Q})} = -\alpha e^{-\mu r}/r$ was proposed to parameterize the interaction between a heavy quark-antiquark pair and the nucleon, with μ and α characterizing the inverse range and strength. Related attractive interactions have also been discussed in terms of soft-gluon exchange or two-pion exchange mechanisms, and have been explored in lattice QCD studies of nucleon-quarkonium systems [3–12]. These studies provide insights into possible OZI-suppressed interactions, whereas the present work focuses on a distinct threshold-driven mechanism relevant to the $N\phi$ system.

Motivated by earlier studies of nucleon-quarkonium interactions, analogous mechanisms have been explored for the $N\phi$ system by replacing the heavy quark pair with an $s\bar{s}$ configuration. For this reason, a possible $N\phi$ bound state was first suggested in Ref. [13] by varying the parameters α and μ in the effective Yukawa potential $V_{(Q\bar{Q})}$. Over the past two decades, the $N\phi$ interaction has been investigated using a variety of approaches, including quark models [14–17], coupled-channel analyses [18–20], lattice QCD simulations [21], and correlation-function analyses on both the theoretical and experimental sides [22–25].

Recent lattice QCD studies indicate that in the $^4S_{3/2}$ channel, inelastic transitions such as $N\phi \rightarrow \Sigma\pi K$ and $\Lambda\pi K$ are suppressed, and coupled-channel effects from ΣK^* and ΛK^* do not play a dominant role in determining the scattering length, yielding $a =$

$-1.43(23)_{\text{stat}}^{(+36)}_{(-06)} {}_{\text{syst}} \text{ fm}$ [21]. An attractive interaction is also indicated by femtoscopy analyses from the ALICE collaboration, where a complex scattering length is extracted as $a = -(0.85 \pm 0.34_{\text{stat}} \pm 0.14_{\text{syst}}) - i(0.16 \pm 0.10_{\text{stat}} \pm 0.09_{\text{syst}}) \text{ fm}$ [25].

Despite these advances, the underlying mechanism responsible for the $N\phi$ interaction remains model dependent and is still under debate [22–24, 26, 27]. This motivates investigation of dynamical origins, in particular those associated with $K\bar{K}$ threshold effect.

From a theoretical perspective, low-energy scattering processes are naturally described in terms of scattering amplitudes, where different dynamics manifest themselves through their characteristic analytic structures. At the tree level, the $N\phi$ interaction is modeled by meson exchange, involving pseudoscalar, scalar, and vector mesons. For pseudoscalar-meson exchange, the contribution is expected to be suppressed due to the small mixing angle between the η and η' mesons. In the case of scalar-meson exchange, although non-singlet σ components may couple to strange quarks [28, 29], the singlet-octet mixing in the scalar sector is known to deviate from the ideal limit that would separate strange and non-strange components [30]. As a result, scalar exchange in the $N\phi$ channel is tiny due to the small SU(3) broken effect. For vector-meson exchange, the small $\omega\phi$ mixing angle, $\epsilon_{\omega\phi} = 0.0549$ [31], further constrains the possible strength of the interaction. Moreover, when the spin-spin component is attributed to be subleading relative to the spin-independent part, the interaction is expected to be weak and perturbative in the near-threshold region.

At the loop level, contributions beyond tree-level meson exchange may also arise. By analogy with the two-pion-exchange mechanism studied in $J/\psi N$ scattering [7, 8], two-pion exchange has been considered in $N\phi$ scattering and incorporated into the interaction potential within the HAL QCD [21], following the structure discussed in Ref. [32]. The two-pion-exchange contribution is evaluated through loop diagrams constructed from meson-baryon amplitudes. However, the leading-

*Electronic address: yanmj0789@swu.edu.cn

†Electronic address: ancs@swu.edu.cn

‡Electronic address: crdeng@swu.edu.cn

order Weinberg-Tomozawa interaction in chiral perturbation theory vanishes in $\phi\pi \rightarrow \phi\pi$ transition [33]. Therefore, two-pion exchange in $N\phi$ scattering originates from subleading chiral interactions and is expected to be suppressed in the low-energy region.

Beyond the two-pion-exchange in $J/\psi N$ scattering, corrections from open-charmed hadron loops, represented by triangle diagrams, are considered in Ref. [4]. Given that, the coupling of the J/ψ to $D\bar{D}$ is suppressed compared to the $\phi K\bar{K}$ coupling, with a ratio $R_1 \simeq 1/4$. In addition, the DN interaction near threshold is weaker than the πN interaction, leading to a ratio $R_2 \simeq 0.1$. In the strange sector, these suppression factors are naturalness. The $\phi K\bar{K}$ coupling is unsuppressed, corresponding to $R_1 \sim \mathcal{O}(1)$, while the Weinberg-Tomozawa interaction enhances the $N\bar{K}$ amplitude relative to πN by a factor proportional to m_K/m_π . Furthermore, the proximity of the ϕ mass to the $K\bar{K}$ threshold induces a kinematical enhancement in the loop integral, which can be evaluated by a factor of $(m_{J/\psi} - 2m_D)^2 / (m_\phi - 2m_K)^2$ when compared to the corresponding D -meson loop. These considerations indicate that triangle-diagram contributions associated with the $K\bar{K}$ threshold are enhanced in the $N\phi$ system. In particular, the proximity of the $K\bar{K}$ threshold, together with the presence of near-threshold structures in the $N\bar{K}$ subsystem, promotes the loop amplitude through both kinematics and dynamics. As a consequence, the triangle diagram provides an effective interaction with a range of $1/\sqrt{m_K(m_\phi - 2m_K)}$. Such loop-induced mechanisms are expected to play a non-negligible role in low-energy $N\phi$ scattering and contribute to the scattering length within the framework of the effective-range expansion. In addition, a characteristic threshold scaling behavior as a smoking-gun signal of three-body dynamics is encoded in the pole-enhanced triangle diagram.

This article is organized as follows. In Sec. II, the effective-range expansion for low-energy $N\phi$ scattering associated with triangle-diagram contributions from two-kaon exchange is introduced. In Sec. III, the behavior of the $N\phi$ scattering length is presented and compared with results from HAL QCD and femtoscopic analyses by the ALICE collaboration. A summary and outlook are given in Sec. IV.

II. FORMALISM

In the non-relativistic description of low-energy $N\phi$ scattering, the effective potential is introduced as

$$V = c_0 + d_0 \langle N | \vec{\sigma} \cdot \vec{k} | N \rangle \langle \phi | \vec{S}_1 \cdot \vec{k} | \phi \rangle = c_0 + \frac{1}{2} d_1^{\frac{1}{2}, \frac{3}{2}} \vec{k}^2 \quad (1)$$

where $\vec{\sigma}$ and \vec{S}_1 denote the Pauli matrices and the spin-1 operator, respectively, and \vec{k} is the three-momentum of the nucleon in the center-of-mass frame. The c_0 represents the spin-independent (or spin-averaged) interac-

tion, while $d_1^{\frac{1}{2}, \frac{3}{2}}$ parameterizes the spin-dependent contribution for total spin 1/2 and 3/2, respectively.

In the vicinity of the $N\phi$ threshold, where $\vec{k}^2 \rightarrow 0$, the inverse potential is expanded as

$$\frac{1}{V} = \frac{1}{c_0} \frac{1}{1 + \frac{1}{2} \frac{d_1^{\frac{1}{2}, \frac{3}{2}}}{c_0} \vec{k}^2} \simeq \frac{1}{c_0} \left(1 - \frac{1}{2} \frac{d_1^{\frac{1}{2}, \frac{3}{2}}}{c_0} \vec{k}^2 \right), \quad (2)$$

so that, at leading order in the threshold expansion, the spin-dependent correction enters only at $\mathcal{O}(\vec{k}^2)$ and is subleading.

The low-energy scattering amplitude is parameterized in the effective-range expansion,

$$\frac{8\pi th}{T} = V^{-1} - G = -\frac{1}{a^{\frac{1}{2}, \frac{3}{2}}} - ik, \quad (3)$$

where $th = m_N + m_\phi$, V denotes the effective potential, and $G = -\Lambda_0^{\frac{1}{2}, \frac{3}{2}}/\pi + ik$ is the two-point loop function regularized by the cutoff Λ_0 [34]. The corresponding scattering lengths are given by $a^{\frac{1}{2}, \frac{3}{2}} = -1/\left(1/c_0 + \Lambda_0^{\frac{1}{2}, \frac{3}{2}}/\pi\right)$.

When $\Lambda_0^{\frac{1}{2}, \frac{3}{2}}$ are truncated at the same scale, which is concerned here, $a^{\frac{1}{2}, \frac{3}{2}}$ are degenerated to be a , where the contribution from the spin-dependent interaction to the scattering length is attributed to be subleading [35, 36] and not considered in the present study. The scattering length a is a real quantity in a single-channel description, while it generally becomes complex once coupled-channel effects from inelastic channels below the $N\phi$ threshold are taken into account.

The $N\phi$ interaction can be conveniently decomposed into contributions from different dynamics,

$$V = V_{\text{oth.}}(\Lambda_1) + V_{\text{tri.}}(\Lambda_2), \quad (4)$$

where $V_{\text{tri.}}$ denotes the contribution associated with the triangle diagram, while $V_{\text{oth.}}$ collects short-range interactions. The two terms are characterized by different renormalization scales, Λ_1 and Λ_2 , reflecting their distinct dynamical origins. Here, Λ_1 represents a relatively hard scale associated with short-distance physics, whereas Λ_2 corresponds to a softer scale relevant for loop contributions near the $K\bar{K}$ threshold.

At high energy scale, generically denoted by Λ_1 , short-range interactions contained in $V_{\text{oth.}}$ are expected to provide the dominant interaction. We do not intend to model the full $N\phi$ interaction in a large energy range, but rather to isolate and quantify the threshold-driven dynamics that becomes prominent in the low-energy region around Λ_2 . In this window, the triangle mechanism represents the leading nonperturbative contribution, while $V_{\text{oth.}}$ is much smaller than the $V_{\text{tri.}}$ and enters as a subleading short-distance correction, which can be referred to the renormalization group evolution [37–39] stemming from the Langer correction [40].

The relative size of short-range contributions can be obtained from scale separation and EFT power counting. The triangle diagram is characterized by a long-range scale $r_{\text{tri}} \sim 1/\sqrt{m_K|\delta|}$ from the near-threshold Kaon loop, whereas short-range interactions are governed by $r_{\text{oth}} \sim 1/\Lambda_\chi$ with $\Lambda_\chi \sim 1.0 \text{ GeV}$. Since the scattering length is dominated by distances $r \sim 1/k_{\text{eff}}$ and is governed by the spatial integral of the interaction, one expects

$$\frac{a_{\text{oth}}}{a_{\text{tri}}} \sim \left(\frac{r_{\text{oth}}}{r_{\text{tri}}} \right)^1 \text{ or } \left(\frac{r_{\text{oth}}}{r_{\text{tri}}} \right)^3$$

implying a strong suppression of short-range interactions in the near-threshold regime, where the powers 1 and 3 correspond to the behavior of the triangle diagram in low-energy scattering. This is consistent with EFT power counting, where the triangle mechanism is infrared enhanced by the near-threshold momentum scale, while short-range interactions enter through local operators suppressed by the hard scale Λ_χ . Thus, although short-distance physics can renormalize the overall strength, the threshold behavior of the scattering length is governed by the pole-enhanced triangle mechanism.

Such a separation of scales provides a useful framework for organizing the low-energy interaction, in which contributions from V_{oth} are treated perturbatively around the threshold-sensitive dynamics encoded in V_{tri} . This hierarchy applies only within a narrow momentum window characterized by a low scale Λ_2 , which is set by the proximity to the $K\bar{K}$ threshold and by the near-threshold structure in the $N\bar{K}$ subsystem.

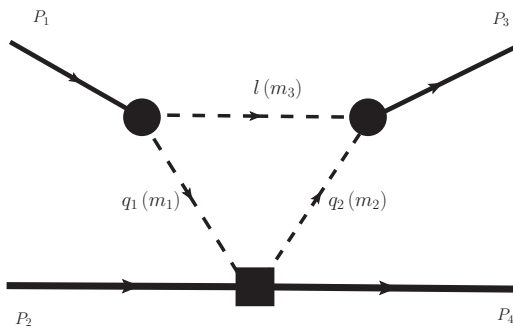


FIG. 1: Schematic illustration of the two-kaon-exchange contribution to $N\phi$ scattering through a triangle diagram. The dashed, solid, and bold lines represent the kaon, ϕ meson, and nucleon, respectively. The corresponding particle mass and momentum are labeled in the figure.

The term V_{tri} corresponds to the two-kaon-exchange contribution represented by the triangle diagram shown in Fig. 1. This diagram involves two types of interaction vertices: (i) the coupling of the ϕ meson to a $K\bar{K}$

pair, and (ii) elastic $NK(\bar{K})$ scattering. The former is described by a vector-pseudoscalar-pseudoscalar interaction, with the effective Lagrangian given by

$$\mathcal{L}_{\phi K\bar{K}} = ig \phi^\mu (\bar{K} \partial_\mu K - K \partial_\mu \bar{K}), \quad (5)$$

where the coupling constant is fixed by $g = m_V/(2F_\pi) = 4.20$, with $m_V = m_\rho = 775 \text{ MeV}$ and $F_\pi = 92.1 \text{ MeV}$.

The low-energy NK and $N\bar{K}$ interactions entering the triangle diagram are estimated in chiral perturbation theory. At leading order, the vertex of the pseudoscalar meson scattering off the octet baryon is described by the Weinberg-Tomozawa interaction,

$$\mathcal{L}_{WT} = \left\langle \bar{B} i\gamma^\mu \frac{1}{4F_\pi^2} [[\Phi, \partial_\mu \Phi], B] \right\rangle. \quad (6)$$

where Φ and B denote the SU(3) matrices for the pseudoscalar mesons and baryons, respectively,

$$\Phi = \begin{pmatrix} \frac{1}{\sqrt{2}}\pi^0 + \frac{1}{\sqrt{6}}\eta & \pi^+ & K^+ \\ \pi^- & -\frac{1}{\sqrt{2}}\pi^0 + \frac{1}{\sqrt{6}}\eta & K^0 \\ K^- & \bar{K}^0 & -\frac{2}{\sqrt{6}}\eta \end{pmatrix}, \quad (7)$$

$$B = \begin{pmatrix} \frac{1}{\sqrt{2}}\Sigma^0 + \frac{1}{\sqrt{6}}\Lambda & \Sigma^+ & p \\ \Sigma^- & -\frac{1}{\sqrt{2}}\Sigma^0 + \frac{1}{\sqrt{6}}\Lambda & n \\ \Xi^- & \Xi^0 & -\frac{2}{\sqrt{6}}\Lambda \end{pmatrix}. \quad (8)$$

This interaction leads to a low-energy structure of the form $\bar{u} \gamma_\mu (k_1^\mu + k_2^\mu) u$ for the elastic $NK(\bar{K})$ channels, where u and \bar{u} are Dirac spinors and k_1 and k_2 denote the four-momenta of the incoming and outgoing mesons.

The numerator of the loop amplitude $I(l)$ associated with the triangle diagram in Fig. 1 is written as

$$\begin{aligned} \text{Num} &= g_{\text{eff}} \epsilon^\mu (2l - P_1)_\mu (2l - P_3)_\nu \epsilon^\nu u(P_2) \bar{u}(P_4) \\ &= g_{\text{eff}} \vec{\epsilon} \cdot \vec{\epsilon}' (2\vec{l} - \vec{P}_1) \cdot (2\vec{l} - \vec{P}_3) u(P_2) \bar{u}(P_4) \\ &= g_{\text{eff}} [4\vec{l}^2 + \vec{P}_1 \cdot \vec{P}_3] u(P_2) \bar{u}(P_4), \end{aligned} \quad (9)$$

where g_{eff} denotes the product of the coupling constants at the interaction vertices. In non-relativistic $N\phi$ scattering, the intermediate kaons propagate close to their mass shell, such that $l^0 - m_K \sim \vec{l}^2/(2m_K) \ll m_K$.

The loop amplitude is decomposed into partial waves of the $N\phi$ system. Near threshold, the S-wave component gives the leading contribution to the scattering amplitude, while higher partial waves are suppressed by additional powers of the external momenta. In particular, the D-wave contribution enters at higher order in the threshold expansion and does not contribute to the scattering length.

The S-wave projected amplitude $I(l)$ is

$$\begin{aligned}
I(l) &= \int \frac{d^4 l}{(2\pi)^4} \frac{-g_{\text{eff}} \left[4\vec{l}^2 + \vec{P}_1 \cdot \vec{P}_3 \right] u(P_2) \bar{u}(P_4)}{(l^2 - m_1^2) \left[(P_1 - l)^2 - m_2^2 \right] \left[(P_3 - l)^2 - m_3^2 \right]} \\
&= \int \frac{d^4 l}{(2\pi)^4} \frac{-g_{\text{eff}}}{8\omega_1 \omega_2 \omega_3} \frac{4\vec{l}^2 + \vec{P}_1 \cdot \vec{P}_3}{l^0 - \omega_1 + i\epsilon} \frac{u(P_2) \bar{u}(P_4)}{P_1^0 - l^0 - \omega_2 + i\epsilon} \frac{1}{P_3^0 - l^0 - \omega_3 + i\epsilon},
\end{aligned} \tag{10}$$

where $m_1 = m_2 = m_3 = m_K$ and the energies of the intermediate kaons are approximated as

$$\begin{aligned}
\omega_1 &= m_K + \frac{\vec{l}^2}{2m_K}, \\
\omega_2 &= m_K + \frac{(\vec{P}_1 - \vec{l})^2}{2m_K}, \\
\omega_3 &= m_K + \frac{(\vec{P}_3 - \vec{l})^2}{2m_K},
\end{aligned} \tag{11}$$

which implies the integration over the component l^0 is convergent, and can be evaluated by contour integration.

Near the $N\phi$ threshold, the intermediate kaons propagate close to their mass shell, such that $\omega_1 - m_K \rightarrow 0$. The integrand of the loop function develops an 0/0 structure. To extract the finite contribution in this limit, L'Hôpital's rule is applied, leading to

$$\begin{aligned}
\frac{\omega_1 - m_K}{(P_1^0 - \omega_1 - \omega_2)(P_3^0 - \omega_1 - \omega_3)} &= \frac{\omega_1 - m_K}{(P_1^0 - \omega_2)(P_3^0 - \omega_3) + \omega_1^2 - \omega_1(P_1^0 + P_3^0 - \omega_2 - \omega_3)} \\
&\xrightarrow{\omega_1 \rightarrow m_K} \frac{1}{P_1^0 + P_3^0 - 2\omega_1 - \omega_2 - \omega_3} \simeq \frac{1}{P_1^0 - P_3^0 - 4\omega_1}.
\end{aligned} \tag{12}$$

Evaluating the l^0 integral by closing the contour in the lower half of the complex energy plane, the contribution arises from the kaon pole $z_A : l^0 = \omega_1 - i\epsilon$ with the infinitesimal ϵ . The corresponding residue reads

$$\begin{aligned}
2\pi i \text{Res}[I(z_A)] &= \int \frac{d^3 l}{(2\pi)^3} \frac{g_{\text{eff}}}{8m_1 m_2 m_3} \frac{8m_K}{P_1^0 + P_3^0 - 4\omega_1} \\
&+ \int \frac{d^3 l}{(2\pi)^3} \frac{g_{\text{eff}}}{8m_1 m_2 m_3} \frac{\vec{P}_1^2}{P_1^0 - \omega_1 - \omega_2} \frac{1}{P_3^0 - \omega_1 - \omega_3}
\end{aligned} \tag{13}$$

where $P_1^0 - \omega_1 - \omega_2 < 0$ and $P_3^0 - \omega_1 - \omega_3 < 0$, which correspond to the $K\bar{K}$ pair forms a bound state associated with the ϕ meson with the unphysical kaon mass. Consequently, the loop function remains real below the $NK\bar{K}$ threshold.

The second term on the right-hand side of Eq. (13) is proportional to \vec{P}_1^2 and vanishes in the limit $\vec{P}_1^2 \rightarrow 0$. Consequently, only the first term contributes to the leading-order S-wave potential, which reads

$$\begin{aligned}
V_{LO}^s &= - \int_0^\infty \frac{4\pi g_{\text{eff}} d|\vec{l}|}{8\pi^3} \frac{\vec{l}^2 \cdot 8m_K}{8m_1 m_2 m_3 (2m_\phi - 4\omega_1)} \\
&= - \frac{1}{4\pi^2} \frac{m_K}{m_1 m_2 m_3} \int_0^\infty \frac{g_{\text{eff}} \vec{l}^2 d|\vec{l}|}{m_\phi - 2\omega_1},
\end{aligned} \tag{14}$$

where $\omega_1 = m_K + \vec{l}^2/(2m_K)$ has been used.

The momentum integral in Eq. (14) shows a linear ultraviolet (UV) divergence. To regularize this divergence, a hard cutoff Λ is introduced, leading to

$$\begin{aligned}
\int_0^\Lambda \frac{\vec{l}^2 d|\vec{l}|}{m_\phi - 2m_K - \vec{l}^2/m_K} &= \int_0^\Lambda \frac{\vec{l}^2 d|\vec{l}|}{\delta - \vec{l}^2/m_K} \\
&= m_K \int_0^\Lambda \frac{\vec{l}^2 - m_K \delta + m_K \delta}{m_K \delta - \vec{l}^2} d|\vec{l}| \\
&= m_K \left[-\Lambda - \frac{m_K \delta}{\sqrt{-m_K \delta}} \arctan \left(\frac{\Lambda}{\sqrt{-m_K \delta}} \right) \right], \\
&= \tilde{I}^{\text{div.}}(\Lambda) + \tilde{I}^{\text{con.}}(\delta),
\end{aligned} \tag{15}$$

where $\delta = m_\phi - 2m_K$. The first term is linearly divergent in the cutoff Λ . In contrast, the second term is finite and encodes the non-analytic dependence on the difference of the $K\bar{K}$ threshold to ϕ mass to ϕ with unphysical masses in the Table. I. The leading-order potential V_{LO}^s is separated into a divergent piece V^{div} and a convergent piece V^{con} . The divergent contribution depends on the cutoff Λ in the triangle diagram, while the convergent part represents the long-distance contribution from the two-kaon-exchange. Although the numerical value of the V_{LO}^s depends on the choice of regularization scheme, the convergent V^{con} depending on the binding energy δ is regulator-independent.

In addition to employing a momentum cutoff Λ , the

loop integral in Eq. (14) can also be regularized using smooth regulators, such as the monopole or Gaussian form factors. The monopole regulator is expanded as

$$\frac{\Lambda_m^2}{\Lambda_m^2 + \vec{l}^2} = 1 - \frac{\vec{l}^2}{\Lambda_m^2} + \mathcal{O}\left(\frac{\vec{l}^4}{\Lambda_m^4}\right), \quad (16)$$

where Λ_m denotes a hard scale. To leading order in the momentum expansion, this regulator reproduces the behavior of a sharp cutoff up to terms that can be absorbed into higher-order contact interactions.

Alternatively, adopting a Gaussian regulator $\exp(-\vec{l}^2/\Lambda_G^2)$ leads to a simple mapping between the cutoff scales,

$$\Lambda_G = \sqrt{\frac{2}{\pi}} \Lambda, \quad (17)$$

such that the Gaussian and sharp-cutoff schemes yield equivalent results for the leading contribution to the potential.

Since the study focuses on the long-distance dynamics associated with near-threshold kaons, we do not attempt to resolve the origin of the short-distance contributions. Their effects are encoded in local counter-terms whose values must be fixed by external input and therefore do not affect the qualitative threshold behavior in this work. Therefore, the conclusions regarding the role of triangle diagram and the threshold behavior of the $N\phi$ scattering length are not altered by different regularization prescriptions.

The second term on the right-hand side of Eq. (15) is finite and appears in the form of an arctan function. Regarding $g_{\text{eff}} = g^2 V^{WT}$, the Weinberg-Tomozawa interaction enters both the divergent and convergent parts of the loop integral. The divergent part is

$$V^{\text{div}} = -\frac{g^2}{4\pi^2} \frac{m_K^2}{m_1 m_2 m_3} \int_0^\Lambda V^{WT}(|\vec{l}|) d|\vec{l}|, \quad (18)$$

which leads to a sum on permutations of K and \bar{K} in the triangle loop, where the Weinberg-Tomozawa interaction corresponds to the isospin channels

$$V_{I=0, N\bar{K}}^{WT}, \quad V_{I=1, N\bar{K}}^{WT}, \quad V_{I=0, NK}^{WT}, \quad V_{I=1, NK}^{WT}, \quad (19)$$

with the corresponding coefficients -3 , -1 , 0 , and 2 , respectively. The isospin-averaged interactions are given by $V_{N\bar{K}}^{WT} = \frac{1}{2} V_{I=0, N\bar{K}}^{WT} + \frac{1}{2} V_{I=1, N\bar{K}}^{WT}$ and $V_{NK}^{WT} = \frac{1}{2} V_{I=1, NK}^{WT}$.

If dynamically generated poles appear in the $N\bar{K}$ or NK scattering, the Weinberg-Tomozawa interaction should, in principle, be replaced by a resummed series of bubble diagrams, which accounts for multiple rescattering in the corresponding two-body channels [41]. Such a resummation generates near-threshold poles, most notably the $\Lambda(1405)$ in the $N\bar{K}$ scattering, and substantially enhances the triangle amplitude.

To illustrate how these effects enter beyond the Weinberg-Tomozawa vertex, the corresponding two-loop diagrams are shown in Fig. 2. Diagram (a) represents the contribution in which the $N\bar{K}$ (or NK) interaction in the triangle is dressed by the resummed bubble series, giving rise to a dynamically generated pole, whereas diagram (b) corresponds to a non-resonant two-loop correction without such pole enhancement.

Once the bubble resummation is inserted into the triangle diagram, both diagrams (a) and (b) generate ultra-violet divergences of $\mathcal{O}(\Lambda^2)$. These contributions are beyond the renormalization accuracy of the one-loop treatment and must be absorbed into higher-order counter-terms, which is not the focus of this study. Therefore, at order $\mathcal{O}(\Lambda)$, the divergent part V^{div} is consistently evaluated using only the Weinberg-Tomozawa interaction without resummation.

In contrast, the convergent part V^{con} is dominated by low-momentum regions of the loop integration and is sensitive to near-threshold dynamics. In this case, the enhancement induced by the dynamically generated $N\bar{K}$ pole in diagram (a) constitutes a genuine long-distance effect that is retained explicitly, while the contribution from diagram (b) remains subleading and does not involve threshold effect.

As a consequence, the divergent part V^{div} is evaluated with the Weinberg-Tomozawa vertex only, while the effect of the dynamically generated near-threshold pole is incorporated in the convergent part V^{con} . Importantly, introducing the pole through the resummed bubble series modifies only the low-energy behavior of the integrand, and does not alter the convergence of the loop integral in Eq. (15). Therefore, it is not necessary to re-evaluate the full triangle-loop integral with dressed propagators in V^{con} .

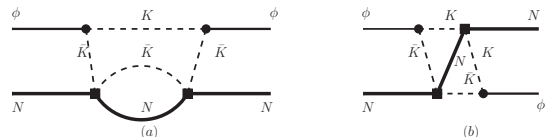


FIG. 2: The $N\phi$ scattering driven by two-loop diagrams with Kaon scattering off nucleon. The dashed, solid, and bold lines represent Kaon, ϕ meson, and N , respectively, where the bubble represents $\mathcal{V} + \mathcal{V}\mathcal{G}\mathcal{V} \dots$ with the Weinberg-Tomozawa interaction \mathcal{V} and $N\bar{K}$ loop \mathcal{G} .

The upper limits of the loop momentum are constrained by the mass at which additional degrees of freedom become relevant. In the case of $N\bar{K}$ rescattering, the $\Lambda(1520)$ resonance is not included explicitly. Accordingly, the loop momentum carried by the \bar{K} in the Weinberg-Tomozawa interaction is restricted by this excitation, leading to $l_{N\bar{K}}^{\text{max}} = 245$ MeV. Similarly, for NK rescattering, the NK^* channel is not included, and the corresponding loop momentum is bounded by the NK^* threshold, $l_{NK}^{\text{max}} = 553$ MeV.

Focusing on $N\phi$ scattering in the vicinity of the

threshold, the momentum dependence of the Weinberg-Tomozawa interaction entering the divergent part V^{div} can be expanded as

$$V^{WT}(|\vec{l}|) = V^{WT}(|\vec{l}|=0) + \mathcal{O}(\delta). \quad (20)$$

The $\mathcal{O}(\delta)$ terms are suppressed in the near-threshold region and are neglected at the present order. As a result, the divergent contribution is written as

$$\begin{aligned} V^{\text{div}} &= -\frac{g^2}{4\pi^2 m_K^2} \tilde{I}^{\text{div}}(\Lambda) V^{WT} \\ &= \frac{g^2}{4\pi^2 m_K} \sum_{i=NK, N\bar{K}} V_i^{WT} \Lambda_i, \end{aligned} \quad (21)$$

where the index i labels the NK and $N\bar{K}$ rescattering processes, with $\Lambda_{NK} = l_{NK}^{\text{max}}$ and $\Lambda_{N\bar{K}} = l_{N\bar{K}}^{\text{max}}$.

Using the relative strengths of the Weinberg-Tomozawa interactions listed in Eq. (19), the divergent part can be expressed as

$$V^{\text{div}} = \frac{g^2 V_{I=0, N\bar{K}}^{WT}}{4\pi^2 m_K} \left(\frac{1}{3} l_{NK}^{\text{max}} - \frac{2}{3} l_{N\bar{K}}^{\text{max}} \right). \quad (22)$$

This expression represents a residual short-distance contribution after partially cancellation among different isospin channels. Numerically, the combination $\frac{1}{3} l_{NK}^{\text{max}} - \frac{2}{3} l_{N\bar{K}}^{\text{max}}$ is smaller than the characteristic low-energy scale $\sqrt{m_K \delta}$ appearing in Eq. (15), indicating that V^{div} remains subleading compared to V^{con} .

As a consequence, the triangle diagram leads to

$$\frac{1}{V^{\text{div}} + V^{\text{con}}} \simeq \frac{1}{V^{\text{con}}} \left(1 - \frac{V^{\text{div}}}{V^{\text{con}}} \right), \quad (23)$$

where the expansion is justified by $|V^{\text{div}}| \ll |V^{\text{con}}|$. The subleading term proportional to $V^{\text{div}}/V^{\text{con}}{}^2$ renormalizes the ultraviolet divergence appearing in the $N\phi$ loop function G in Eq. (3). This renormalization is expressed in terms of an effective subtraction scale $\Lambda_0 = -\pi V^{\text{div}}/V^{\text{con}}{}^2$. According to the parameters adopted in the next section, Λ_0 is found to be about 150 MeV with inputs in Table I, which lies well within the momentum range relevant for near-threshold $N\phi$ scattering. This indicates that the effective-range expansion remains valid here, and that corrections beyond the scattering lengths are suppressed. Accordingly, the $N\phi$ scattering lengths in the spin-1/2 and spin-3/2 channels, which are degenerated at leading order, are approximated as

$$-\frac{1}{a_{N\phi}} = \frac{1}{V^{\text{con}}}. \quad (24)$$

This relation works as long as the typical external momenta are much smaller than the inverse range of the interaction. The scale is associated with the triangle mechanism, so that the momentum expansion underlying the effective-range expansion is justified in the near-threshold region. Consequently, higher-order terms beyond the scattering length, such as the effective-range parameter, are suppressed.

TABLE I: Inputs of the isospin-averaged hadron masses [21]

Hadron	Lattice [MeV]	Expt. [MeV]
K	524.7	495.6
ϕ	1048.0	1019.5
N	954.0	938.9

We emphasize that the present analysis is focused on the threshold behavior of the $N\phi$ amplitude and does not aim at describing possible bound or virtual states close to the threshold, where higher-order terms in the effective-range expansion could become important. Within the kinematic window relevant for the extraction of the scattering length, however, the approximation in Eq. (3) remains reliable.

III. RESULTS AND DISCUSSION

To evaluate the convergent contribution V^{con} , the role of near-threshold poles in the $N\bar{K}$ scattering is considered. In the isoscalar channel, the $\Lambda(1405)$ resonance is widely interpreted as a dynamically generated $N\bar{K}$ bound state [42–47]. The proximity of this pole to the $N\bar{K}$ threshold leads to a significant enhancement of the low-energy $N\bar{K}$ amplitude, which in turn promotes the convergent part of the triangle-diagram contribution to $N\phi$ scattering. In the isovector $N\bar{K}$ channel, a virtual pole has been reported in several analyses and is sometimes associated with a broad Σ excitation around 1.4 GeV [42, 48–51]. This pole is located further from the physical sheet than the $\Lambda(1405)$ and therefore provides a subleading correction to the triangle diagram at threshold. By contrast, the NK interaction in the $I=0$ and $I=1$ channels is governed by a vanishing ($C_{ij}=0$) and a repulsive ($C_{ij}=2$) Weinberg-Tomozawa term, respectively, and does not generate a near-threshold pole. As a result, the NK subsystem does not induce an analogous enhancement of the convergent triangle contribution. These considerations indicate that the near-threshold structure associated with the $\Lambda(1405)$ provides the leading enhancement mechanism for V^{con} , while other channels yield perturbative corrections.

According to the HAL QCD results obtained with an unphysical kaon mass $m_K = 524.7$ MeV, as listed in Table I, the same kaon mass is adopted in the present analysis for consistency. The $K\bar{K}$ threshold lies slightly above the ϕ mass, leading to

$$\delta \equiv m_\phi - 2m_K = -\tilde{\delta} = -1.0(4) \text{ MeV}.$$

This small negative value indicates that the ϕ is marginally bound with respect to the $K\bar{K}$ threshold at the unphysical mass point, which enhances the near-threshold sensitivity of the triangle diagram.

The use of an unphysical kaon mass also induces a corresponding modification of the $\phi K\bar{K}$ coupling constant g . Invoking $SU(3)$ flavor symmetry, this coupling

is related to the $\rho\pi\pi$ coupling, $g_{\rho\pi\pi}$, governing the decay $\rho \rightarrow \pi\pi$. The pion-mass dependence of this coupling can be parametrized as

$$g_{\rho\pi\pi} = \tilde{c}_0 + \tilde{c}_1 m_\pi^2.$$

Lattice and phenomenological studies show that $g_{\rho\pi\pi}$ varies only mildly, at the level of 2%–4%, when the pion mass is varied from 140 to 200 MeV [52], in agreement with earlier analyses indicating an approximate pion-mass independence of this coupling [53, 54]. Consequently, the modification of the $\phi\bar{K}\bar{K}$ coupling induced by the unphysical light-quark masses is expected to be numerically small and does not affect the qualitative features of the near-threshold $N\phi$ interaction discussed below.

Subsequently, the leading-order S-wave potential induced by the triangle diagram is estimated analytically as

$$V_{LO}^s = \frac{3g^2 R_{\text{pole}}}{4F_\pi^2} \sqrt{m_K \tilde{\delta}} \arctan\left(\frac{\Lambda}{\sqrt{m_K \tilde{\delta}}}\right), \quad (25)$$

which is a scalar quantity and provides the large contribution to the $N\phi$ scattering length. The factor R_{pole} parametrizes the relative enhancement of the triangle amplitude induced by the near-threshold $\Lambda(1405)$ pole compared to the leading-order Weinberg-Tomozawa interaction,

$$R_{\text{pole}} = \frac{g_i^2 / |th_{N\bar{K}} - \sqrt{s_{\text{pole}}}|}{V^{WT}} = 5.65^{+1.13}_{-0.96}, \quad (26)$$

with the $N\bar{K}$ threshold $th_{N\bar{K}}$, where $\sqrt{s_{\text{pole}}}$ denotes the pole position of the $\Lambda(1405)$, and the coupling g_i is taken from Ref. [55]. The quoted uncertainty reflects the difference between the Fit-I and Fit-II parameterizations.

It is worth emphasizing that the pole contribution is qualitatively different from a local contact interaction such as V^{WT} . Owing to the proximity of the $\Lambda(1405)$ pole to the $N\bar{K}$ threshold and its strong coupling to the $N\bar{K}$ channel, the corresponding amplitude shows a pronounced energy dependence as the center-of-mass energy approaches $\sqrt{s_{\text{pole}}}$. Although s_{pole} is complex, the $\Lambda(1405)$ remains relatively narrow and dominantly couples to the $N\bar{K}$ channel, while its couplings to other channels are not dominant [42–47].

In the low-energy $N\phi$ scattering, the kinematics constrain the intermediate $N\bar{K}$ subsystem to energies close to the $N\bar{K}$ threshold. The enhancement induced by the $\Lambda(1405)$ pole is captured by the factor R_{pole} , which governs the main contribution of the $N\bar{K}$ rescattering to the triangle diagram.

The numerical results for the $N\phi$ scattering length are obtained by varying the binding energy of the intermediate $K\bar{K}$ system to the ϕ meson. The corresponding results are shown in Fig. 3. The calculated curves show good agreement with the magenta band extracted in the spin-3/2 channel at an unphysical pion mass in Ref. [21],

as well as with the green band corresponding to the spin-averaged scattering length measured by the ALICE collaboration [25].

The uncertainty associated with the enhancement factor R_{pole} , which is determined from the physical parameters and pole couplings, propagates into the prediction of the scattering length. This effect is illustrated in Fig. 4, where the results are presented for the central value of $\tilde{\delta}$, and the uncertainty bands reflect the variation of R_{pole} . The theoretical curves are fully covered by the corresponding uncertainty bands, indicating a stable prediction within the adopted parameter ranges.

These results suggest that the threshold dynamics driven by the two-kaon-exchange triangle diagram, promoted by the near-threshold $\Lambda(1405)$ pole in the $N\bar{K}$ scattering, provides a natural and consistent explanation of the observed $N\phi$ scattering length.

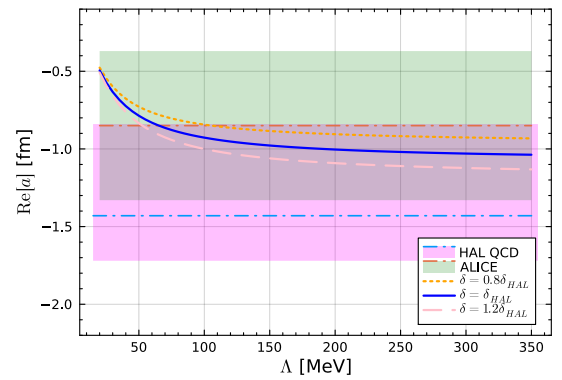


FIG. 3: The $N\phi$ scattering length from two-Kaon-Exchange with $\tilde{\delta} = (1.0 \pm 0.2)$ MeV, where the solid, dashed, and dotted lines correspond to the central value, lower and upper limits of δ , respectively. The magenta and green bands represent the real part of the scattering lengths from HAL QCD [21] and ALICE collaboration [25], respectively.

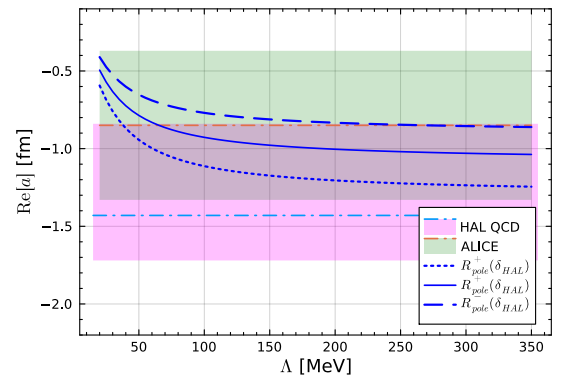


FIG. 4: The $N\phi$ scattering length from two-Kaon-Exchange with uncertainty in R_{pole} deduced by physical couplings.

Concerning the use of physical couplings in $V^{\text{con.}}$, the possible modification of the coupling g_i induced by the

unphysical hadron masses is estimated at the order-of-magnitude level by a mass extrapolation,

$$\frac{g_i^{\text{unphy.} 2}}{g_i^2} \simeq \left(\frac{m_N^{\text{unphy.}}}{m_N} \right)^2 \left(\frac{m_K^{\text{unphy.}}}{m_K} \right)^2 \approx 1.19, \quad (27)$$

which serves only as an indicative estimate. A quantitative determination of this dependence would require dedicated lattice QCD input and is beyond the scope of this study.

The uncertainty in g_i corresponds to an overall variation of the potential at the level of $\pm 19\%$. As a consequence, the uncertainty bands shown in Fig. 5 are comparable to those in Fig. 4, with the dashed and dotted curves remaining within the corresponding error bands. This stability indicates that the triangle-diagram-driven dynamics persists once the quark-mass dependence of the couplings is considered. Therefore, the conclusion on the dominance of the two-kaon-exchange triangle mechanism remains unaffected by reasonable variations of the coupling constants.

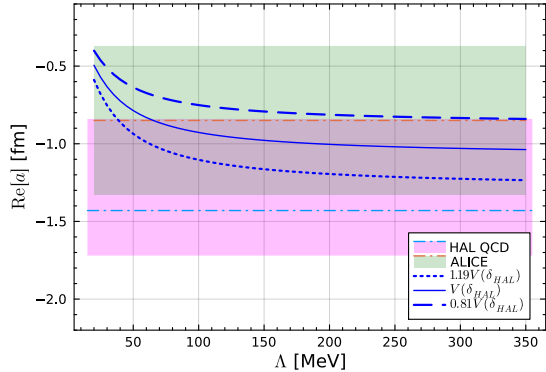


FIG. 5: The $N\phi$ scattering length from two-Kaon-Exchange with uncertainty in g_i .

In addition, the possible modification of the pion decay constant F_π associated with the unphysical kaon mass is taken into account. Following Ref. [56], it is parameterized as

$$F_\pi^{\text{unphy.}} = F_\pi^{\text{phy.}} (1 + r_{F_\pi} \Delta m^2), \quad (28)$$

with $\Delta m^2 = m_K^{\text{phys.} 2} - m_K^2$ and $r_{F_\pi} = 0.53 \text{ GeV}^{-2}$, as extracted from the *BE14extract* shown in Fig. 4 of Ref. [56]. Around the physical kaon mass, the *free-fit* results show a smooth behavior, leading to a correction of less than 1% in F_π . Such a small effect is therefore treated as a higher-order perturbative correction. The associated uncertainty is estimated through Eq. (28) as

$$(1 + r_{F_\pi} \Delta m^2)^{-n_0} = 1.00 (-0.03) (-0.06), \quad (29)$$

where $n_0 = 2$ and 4 correspond to the cases in which the coupling g is taken to be independent of, or dependent of, F_π , respectively.

The variations of the potential translate into the scattering lengths shown in Fig. 6, where the dashed and dotted curves indicate the corresponding upper and lower limits. These curves remain within the cutoff-variation bands for $\Lambda \in [20, 300] \text{ MeV}$, demonstrating a good numerical convergence. The narrow separation between the dashed and dotted curves further confirms that the pion-mass dependence of F_π is perturbative. Therefore, the uncertainty associated with the light-quark-mass dependence of F_π does not affect the conclusions.

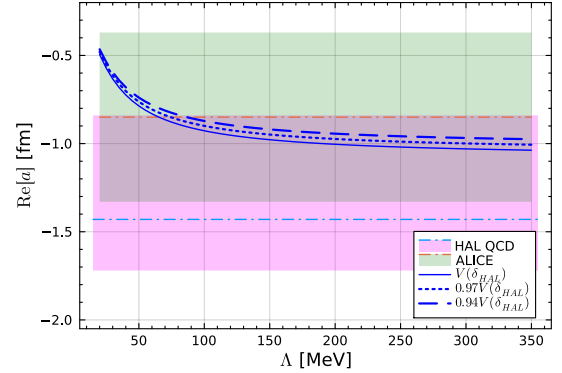


FIG. 6: The $N\phi$ scattering length from two-Kaon-Exchange with uncertainty in F_π , where the solid, dashed, and dotted lines correspond to the central value, lower, and upper limits of $n_0 = 0, 2, 4$, respectively.

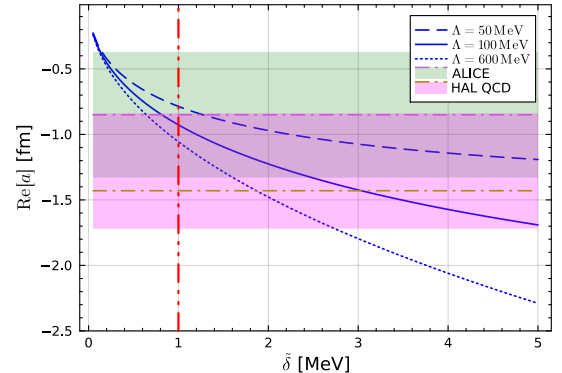


FIG. 7: The $N\phi$ scattering length from Two-Kaon-Exchange with choices on $\tilde{\delta}$, where the solid, dashed and dotted lines correspond to the central value, lower and upper limits of δ , respectively.

In Fig. 7, the dependence of the cutoff Λ in the triangle loop is examined in the evaluation of the $N\phi$ scattering length. The cutoff window is chosen as $\Lambda \in [50, 600] \text{ MeV}$, which safely covers the maximal loop momenta l_{NK}^{max} and $l_{N\bar{K}}^{\text{max}}$ associated with the onset of higher channels and excited resonances. This range is therefore interpreted as a conservative estimate of the residual short-distance uncertainty rather than an additional model parameter. The vertical dash-dot-dot line indi-

cates the meson masses adopted in the HAL QCD simulation [21]. In the small- $\tilde{\delta}$ region, corresponding to the mass difference of $K\bar{K}$ threshold to the ϕ mass, the results show good stability against variations of Λ and show consistent agreement with the lattice-QCD bands. This behavior supports the threshold-enhanced triangle mechanism plays a non-negligible role in the low-energy regime. At larger values of $\tilde{\delta}$, deviations emerge for the largest cutoff $\Lambda = 600$ MeV with $\arctan(\Lambda/\sqrt{m_K \tilde{\delta}})$ being towards to $\frac{\pi}{2}$, where the loop momentum in the triangle diagram is not small anymore and effective-range corrections in the $N\phi$ system—are expected to become relevant. The higher-order contribution goes beyond the leading-order threshold analysis presented here and is deferred to future work.

Beyond the overall agreement of the scattering length with lattice-QCD and femtoscopy results, a particularly distinctive feature of the present analysis is the threshold behavior of the leading-order potential V_{LO}^s . Near the $N\phi$ threshold, V_{LO}^s shows a power-law dependence on the the difference of the $K\bar{K}$ threshold to ϕ mass $\tilde{\delta}$, with $V_{LO}^s \propto \tilde{\delta}^n$. The exponent interpolates between $n = 0$ for small cutoff values and $n = 1/2$ for large cutoffs, reflecting the interplay between the near-threshold kinematics and the loop momentum region probed by the triangle diagram. This behavior is different from that expected for long-range interactions. In particular, the QCD van der Waals force generated by multi-gluon exchange leads to a much steeper dependence, $V \propto \delta^3$ or $\delta^{7/2}$ (equivalently $p_{N\phi}^6$ or $p_{N\phi}^7$) [57, 58]. The power-law scaling found here also differs from that associated with one-boson-exchange descriptions or Yukawa-type interactions [19], and can be further tested in the three-body system [59].

In the case $n = 0$, which corresponds to a small cutoff Λ , the $N\phi$ scattering length becomes only weakly dependent on the difference of the $K\bar{K}$ threshold to ϕ mass. This behavior indicates that the system approaches a regime dominated by near-unitary three-body $NK\bar{K}$ dynamics, in which the characteristic length scale is set by the large scattering length rather than by the range of the underlying interaction. Such a regime provides a particularly sensitive window to three-body correlations, which may act as an ultra-long-range component of the effective interaction.

In this extreme low-energy limit, subleading effects—such as electromagnetic interactions among hadrons—may become comparatively more relevant than in typical hadronic systems, as discussed in Refs. [60–64]. Their quantitative impact, however, depends on the proximity to the unitary regime and requires a dedicated analysis beyond the scope of this study.

For $n = 1/2$, realized for larger cutoff values, the $N\phi$ scattering length shows an approximately linear dependence on the mass difference between the ϕ meson and the $K\bar{K}$ threshold. Both regimes highlight the sensitivity of the $N\phi$ interaction to threshold kinematics and three-body dynamics. A systematic exploration of these

behaviors calls for high-precision scattering data and is well-suited for future lattice-QCD simulations with variations of the light-quark masses. In this sense, the $N\phi$ system offers a rare example in which threshold three-body dynamics leaves a direct imprint on a two-body observable.

On the other hand, for physical hadron masses one finds $\sqrt{m_K |\tilde{\delta}|}/m_K \simeq 0.24$, indicating that the kaons propagating in the triangle diagram remain non-relativistic. This provides a self-consistency check for the expansion in Eq. (25) and motivates an evaluation of the $N\phi$ scattering length using physical masses. The real part of the scattering length is shown in Fig. 8, where the momentum carried by the outgoing Kaon is $|\vec{k}_K| = 118.17$ MeV.

Kinematical consistency requires the cutoff Λ in the loop integral to be larger than the typical momentum flowing through the kaon lines. For a small cutoff value, $\Lambda = 120$ MeV, noticeable deviations from the uncertainty bands are observed. In contrast, for $\Lambda = 300$ –500 MeV the real part of the $N\phi$ scattering length remains stable and overlaps with the bands, supporting the relevance of the triangle mechanism in the physical-mass case.

The scattering lengths are consistent with the real parts obtained in spin-resolved analyses, including the spin-1/2 result of Ref. [22], the spin-3/2 results of Refs. [21, 23, 26], as well as the spin-averaged extraction by the ALICE collaboration [25]. They differ from estimates that include strong coupled-channel effects in the correlation-function approach [27]. Clarifying the origin of these differences among various model descriptions [22, 23, 26] will require further experimental input and refined analyses.

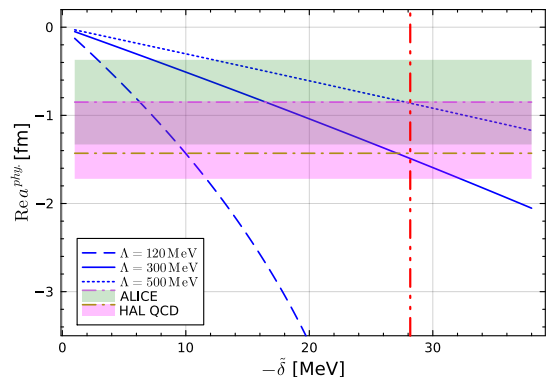


FIG. 8: The real part of the $N\phi$ scattering length from Two-Kaon-Exchange with physical masses, where the solid, dashed, and dotted lines correspond to the central value, lower and upper limits of δ , respectively. The vertical dash-dot-dot line represents the physical ϕ mass with respect to $K\bar{K}$ threshold.

The effectiveness of the triangle-diagram mechanism in $N\phi$ scattering can be traced back to a set of well-defined dynamical conditions. First, there is no interac-

tion channel dominated by a conventional one-particle-exchange contribution at low energies. Second, the two-pion-exchange contribution in the two-point loop is suppressed, owing to the vanishing of the leading-order $\phi\pi \rightarrow \phi\pi$ Weinberg-Tomozawa interaction and weak interactions from other diagrams (see Appendix). Third, the intermediate particles in the triangle diagram propagate close to their mass shells, and the presence of a near-threshold pole in the $N\bar{K}$ subsystem further enhances the amplitude. Together, these features single out the two-kaon-exchange triangle diagram as the dominant low-energy mechanism.

Such threshold-enhanced triangle dynamics is not unique to the $N\phi$ system and has been widely discussed in heavy exotic hadrons. Representative examples include the role of $D\bar{D}$ rescattering in $D\bar{D}\pi$ loops for the $X(3872)$ [65–67], the contribution of $\Sigma_c\bar{D}\pi$ loops to positive-parity $P_c(4457)$ states [68, 69], and the importance of $DD\pi$ loops in the description of the T_{cc} state [70–74]. In these systems, the proximity of two- and three-body thresholds leads to non-perturbative enhancements analogous to those identified here.

A similar mechanism is expected to operate in channels where $D\bar{D}\pi$ couples to $Z_c(4020)$ or $X(4020)$, promoted by the nearby $X(3872)$ or $W_{c1}(3872)$ poles [75, 76]. In such cases, the triangle diagram generates an interaction that plays a role comparable to that of scalar-meson exchange, supplementing the axial-vector exchange mechanism [29]. Related threshold effects have also been discussed for hidden-charm and hidden-strangeness pentaquark states, where the $P_c(4457)$ and $P_{cs}(4560)$ states are enhanced by lower-lying $P_c(4312)$ and $P_{cs}(4338)$ poles through $\bar{D}\Sigma_c\pi$ and $\bar{D}\Xi_c\pi$ loops, respectively [77–87].

Finally, in open-charm pentaquark systems, near-threshold poles in the ND and $N\bar{D}$ channels can further promote the formation of ND^* and $N\bar{D}^*$ states through analogous triangle mechanisms [39, 88, 89]. These examples collectively illustrate that the triangle-diagram mechanism identified in this study represents a generic manifestation of threshold-driven three-body dynamics rather than a system-specific anomaly. The $N\phi$ system thus provides a particularly transparent realization of threshold-enhanced triangle dynamics.

In the dibaryon sector, a closely related dynamical mechanism has been invoked to interpret the $d(2380)$ as a $\Delta\Delta$ molecular state, where the existence of a near-threshold $N\Delta$ bound state plays a crucial role [90]. A similar picture also emerges in the $IJ = 21$ and 12 $N\Delta$ scattering channels when poles in the NN subsystem are taken into account [91]. However, the situation for the $d(2380)$ is considerably more involved: the resonance is located between the $N\Delta\pi$ and $\Delta\Delta$ thresholds, and the large intrinsic width of the Δ renders a clean separation between two-body and three-body dynamics highly non-trivial [39]. This contrasts with the $N\phi$ system, where the thresholds are much better separated and the triangle mechanism can be isolated more transparently.

Another instructive comparison is provided by the $p\Omega$

system, for which a bound state has been reported by the HAL QCD collaboration [92, 93]. When the Ω couples to the $\Xi\bar{K}$ channel, a triangle diagram naturally enters the $p\Omega$ interaction, bearing qualitative similarity to the mechanism discussed for $N\phi$ scattering. A crucial difference is that the Ξ and \bar{K} lines in the triangle diagram are no longer interchangeable. As a result, the ultraviolet divergence in the loop integral cannot be eliminated by symmetry and is instead tied to coupled-channel dynamics [94]. This feature leads to a stronger attractive interaction in the $p\Omega$ system than in the $N\phi$ case. In the meantime, the comparison suggests that the attraction generated by a convergent triangle diagram alone is insufficient to form a bound state at an unphysical kaon mass around 500 MeV.

In the light-meson sector, a pronounced enhancement has been observed near the $\omega\phi$ threshold [95, 96]. This structure may plausibly be driven by a $K_1(1270)\bar{K}$ triangle loop, given that the ωK interaction vanishes at leading order in the Weinberg-Tomozawa interaction. Such a threshold mechanism provides a complementary perspective on the origin of the enhancement and may offer new insight into the long-standing discussion of the glueball-like nature of the $f_0(1710)$.

IV. SUMMARY

In summary, a triangle diagram promoted by the near-threshold $\Lambda(1405)$ is introduced to describe the $N\phi$ scattering in the absence of direct spin interactions. The scattering length, estimated from the convergent part of the triangle diagram with a single cutoff parameter Λ in the triangle loop integral, is found to be consistent with the lattice QCD results from the HAL QCD collaboration [21]. Following the analytic expression deduced from the triangle diagram, the real part of the $N\phi$ scattering length evaluated with physical hadron masses shows a clear overlap with the experimental extraction by the ALICE collaboration [25].

In the low-energy region, the triangle loop integral leads to a power-law dependence of the scattering length on the difference of the $K\bar{K}$ threshold to ϕ mass, $\tilde{\delta}^{0,1/2}$. This behavior indicates that the interaction driven by the promoted triangle diagram is different from both the Van der Waals force [57, 58] and the long-range tail of two-pion exchange [21]. Such a nontrivial power counting reflects the interplay between two-body and three-body dynamics near threshold.

The same dynamical mechanism may also be relevant for understanding other hadronic systems, such as $P_c(4457)$, $Z_c(4020)/X(4020)$, $d(2380)$, and the glueball candidate $f_0(1710)$, where near-threshold poles and intermediate three-body states play an essential role.

Overall, the interaction driven by a promoted triangle diagram provides a unified framework to connect low-energy two-body scattering with underlying three-body dynamics. This mechanism offers a complementary per-

spective on hadron spectroscopy in the nonperturbative regime and can be further tested with future experimental measurements and high-precision lattice QCD simulations.

Acknowledgement

We would like to thank Ju-Jun Xie, Xu Zhang, and Y. Lyu for the fruitful discussions. This research is

supported by the National Natural Science Foundation of China under Grant No. 12305096, the Fundamental Research Funds for the Central Universities under Grant No. SWU-XDJH202304, No. SWU-KQ25016 and Chongqing Natural Science Foundation under Project No. CSTB2025NSCQ-GPX0516.

[1] M. S. Hussein, C. L. Lima, M. P. Pato, and C. A. Bertulani, Phys. Rev. Lett. **65**, 839 (1990).

[2] S. J. Brodsky, I. A. Schmidt, and G. F. de Teramond, Phys. Rev. Lett. **64**, 1011 (1990).

[3] M. E. Luke, A. V. Manohar, and M. J. Savage, Phys. Lett. B **288**, 355 (1992), hep-ph/9204219.

[4] S. J. Brodsky and G. A. Miller, Phys. Lett. B **412**, 125 (1997), hep-ph/9707382.

[5] F. Klingl, S.-s. Kim, S. H. Lee, P. Morath, and W. Weise, Phys. Rev. Lett. **82**, 3396 (1999), [Erratum: Phys. Rev. Lett. 83, 4224 (1999)], nucl-th/9811070.

[6] A. Sibirtsev and M. B. Voloshin, Phys. Rev. D **71**, 076005 (2005), hep-ph/0502068.

[7] H. Fujii and D. Kharzeev, Phys. Rev. D **60**, 114039 (1999), hep-ph/9903495.

[8] B. Wu, X.-K. Dong, M.-L. Du, F.-K. Guo, and B.-S. Zou (2024), 2410.19526.

[9] K. Yokokawa, S. Sasaki, T. Hatsuda, and A. Hayashigaki, Phys. Rev. D **74**, 034504 (2006), hep-lat/0605009.

[10] T. Kawanai and S. Sasaki, Phys. Rev. D **82**, 091501 (2010), 1009.3332.

[11] M. Alberti, G. S. Bali, S. Collins, F. Knechtli, G. Moir, and W. Söldner, Phys. Rev. D **95**, 074501 (2017), 1608.06537.

[12] Y. Lyu, T. Doi, T. Hatsuda, and T. Sugiura, Phys. Lett. B **860**, 139178 (2025), 2410.22755.

[13] H. Gao, T. S. H. Lee, and V. Marinov, Phys. Rev. C **63**, 022201 (2001), nucl-th/0010042.

[14] F. Huang, Z. Y. Zhang, and Y. W. Yu, Phys. Rev. C **73**, 025207 (2006), nucl-th/0512079.

[15] J.-J. Xie and F.-K. Guo, Phys. Lett. B **774**, 108 (2017), 1709.01416.

[16] C.-S. An, J.-J. Xie, and G. Li, Phys. Rev. C **98**, 045201 (2018), 1809.04934.

[17] X. Liu, H. Huang, and J. Ping, Phys. Rev. C **98**, 055203 (2018), 1807.03195.

[18] J. He, H. Huang, D.-Y. Chen, and X. Zhu, Phys. Rev. D **98**, 094019 (2018), 1804.09383.

[19] S.-H. Kim, T. S. H. Lee, S.-i. Nam, and Y. Oh, Phys. Rev. C **104**, 045202 (2021), 2108.12039.

[20] B.-X. Sun, Y.-Y. Fan, and Q.-Q. Cao, Commun. Theor. Phys. **75**, 055301 (2023), 2206.02961.

[21] Y. Lyu, T. Doi, T. Hatsuda, Y. Ikeda, J. Meng, K. Sasaki, and T. Sugiura, Phys. Rev. D **106**, 074507 (2022), 2205.10544.

[22] E. Chizzali, Y. Kamiya, R. Del Grande, T. Doi, L. Fabbietti, T. Hatsuda, and Y. Lyu, Phys. Lett. B **848**, 138358 (2024), 2212.12690.

[23] L. M. Abreu, P. Gubler, K. P. Khemchandani, A. Martínez Torres, and A. Hosaka, Phys. Lett. B **860**, 139175 (2025), 2409.05170.

[24] K. Kuroki and T. Hirano, EPJ Web Conf. **316**, 03009 (2025), 2410.01204.

[25] S. Acharya et al. (ALICE), Phys. Rev. Lett. **127**, 172301 (2021), 2105.05578.

[26] A. Kurós, R. Maj, and S. Mrowczynski (2024), 2408.11941.

[27] A. Feijoo, M. Korwieser, and L. Fabbietti (2024), 2407.01128.

[28] F.-Z. Peng, M.-J. Yan, M. Sánchez Sánchez, and M. P. Valderrama, Eur. Phys. J. C **81**, 666 (2021), 2011.01915.

[29] M.-J. Yan, F.-Z. Peng, M. Sánchez Sánchez, and M. Pavón Valderrama, Phys. Rev. D **104**, 114025 (2021), 2102.13058.

[30] J. A. Oller, Nucl. Phys. A **727**, 353 (2003), hep-ph/0306031.

[31] A. Kucukarslan and U.-G. Meißner, Mod. Phys. Lett. A **21**, 1423 (2006), hep-ph/0603061.

[32] J. Tarrús Castellà and G. Krein, Phys. Rev. D **98**, 014029 (2018), 1803.05412.

[33] L. Roca, E. Oset, and J. Singh, Phys. Rev. D **72**, 014002 (2005), hep-ph/0503273.

[34] X.-K. Dong, F.-K. Guo, and B.-S. Zou, Phys. Rev. Lett. **126**, 152001 (2021), 2011.14517.

[35] X.-K. Dong, F.-K. Guo, and B.-S. Zou, Progr. Phys. **41**, 65 (2021), 2101.01021.

[36] X.-K. Dong, F.-K. Guo, and B.-S. Zou, Commun. Theor. Phys. **73**, 125201 (2021), 2108.02673.

[37] M. Pavón Valderrama and D. R. Phillips, Phys. Rev. Lett. **114**, 082502 (2015), 1407.0437.

[38] M. P. Valderrama, Int. J. Mod. Phys. E **25**, 1641007 (2016), 1604.01332.

[39] F.-Z. Peng, M. Sánchez Sánchez, M.-J. Yan, and M. Pavón Valderrama, Phys. Rev. D **105**, 034028 (2022), 2101.07213.

[40] R. E. Langer, Phys. Rev. **51**, 669 (1937), URL <https://link.aps.org/doi/10.1103/PhysRev.51.669>.

[41] J. A. Oller, E. Oset, and A. Ramos, Prog. Part. Nucl. Phys. **45**, 157 (2000), hep-ph/0002193.

[42] J.-X. Lu, L.-S. Geng, M. Doering, and M. Mai, Phys. Rev. Lett. **130**, 071902 (2023), 2209.02471.

[43] J. Bulava et al. (Baryon Scattering (BaSc)), Phys. Rev. Lett. **132**, 051901 (2024), 2307.10413.

[44] J. Bulava et al. (Baryon Scattering (BaSc)), Phys. Rev. D **109**, 014511 (2024), 2307.13471.

[45] F.-K. Guo, Y. Kamiya, M. Mai, and U.-G. Meißner,

Phys. Lett. B **846**, 138264 (2023), 2308.07658.

[46] Z. Zhuang, R. Molina, J.-X. Lu, and L.-S. Geng (2024), 2405.07686.

[47] Y.-B. He, X.-H. Liu, L.-S. Geng, F.-K. Guo, and J.-J. Xie (2024), 2407.13486.

[48] Y. Ma et al. (Belle), Phys. Rev. Lett. **130**, 151903 (2023), 2211.11151.

[49] W.-T. Lyu, S.-C. Zhang, G.-Y. Wang, J.-J. Wu, E. Wang, L.-S. Geng, and J.-J. Xie, Phys. Rev. D **110**, 054020 (2024), 2405.09226.

[50] E. Wang, L.-S. Geng, J.-J. Wu, J.-J. Xie, and B.-S. Zou, Chin. Phys. Lett. **41**, 101401 (2024), 2406.07839.

[51] H.-P. Li, C.-W. Xiao, W.-H. Liang, J.-J. Wu, E. Wang, and E. Oset, Phys. Rev. D **110**, 114018 (2024), 2409.05787.

[52] Z. Wang, D. B. Leinweber, C. Liu, L. Liu, P. Sun, A. W. Thomas, J.-j. Wu, H. Xing, and K. Yu (2025), 2502.03700.

[53] C. Hanhart, J. R. Pelaez, and G. Rios, Phys. Rev. Lett. **100**, 152001 (2008), 0801.2871.

[54] F. K. Guo, C. Hanhart, F. J. Llanes-Estrada, and U. G. Meissner, Phys. Lett. B **703**, 510 (2011), 1105.3366.

[55] Z.-H. Guo and J. A. Oller, Phys. Rev. C **87**, 035202 (2013), 1210.3485.

[56] B. Ananthanarayan, J. Bijnens, and S. Ghosh, Eur. Phys. J. C **77**, 497 (2017), 1703.00141.

[57] T. Appelquist and W. Fischler, Phys. Lett. B **77**, 405 (1978).

[58] N. Brambilla, V. Shtabovenko, J. Tarrús Castellà, and A. Vairo, Phys. Rev. D **95**, 116004 (2017), 1704.03476.

[59] L.-Z. Wen, Y. Ma, L. Meng, and S.-L. Zhu (2025), 2503.11938.

[60] J. Gasser, V. E. Lyubovitskij, and A. Rusetsky, Phys. Rept. **456**, 167 (2008), 0711.3522.

[61] V. Baru, C. Hanhart, M. Hoferichter, B. Kubis, A. Nogga, and D. R. Phillips, Phys. Lett. B **694**, 473 (2011), 1003.4444.

[62] V. Baru, C. Hanhart, M. Hoferichter, B. Kubis, A. Nogga, and D. R. Phillips, Nucl. Phys. A **872**, 69 (2011), 1107.5509.

[63] Z.-H. Zhang and F.-K. Guo, Phys. Rev. Lett. **127**, 012002 (2021), 2012.08281.

[64] P.-P. Shi, Z.-H. Zhang, F.-K. Guo, and Z. Yang, Phys. Rev. D **105**, 034024 (2022), 2111.13496.

[65] L. Dai, F.-K. Guo, and T. Mehen, Phys. Rev. D **101**, 054024 (2020), 1912.04317.

[66] M.-J. Yan, Y.-H. Ge, and X.-H. Liu, Phys. Rev. D **106**, 114002 (2022), 2208.03943.

[67] X.-H. Cao, M.-L. Du, and F.-K. Guo, J. Phys. G **51**, 105002 (2024), 2401.16112.

[68] F.-Z. Peng, J.-X. Lu, M. Sánchez Sánchez, M.-J. Yan, and M. Pavon Valderrama, Phys. Rev. D **103**, 014023 (2021), 2007.01198.

[69] J.-Z. Wu, J.-Y. Pang, and J.-J. Wu, Chin. Phys. Lett. **41**, 091201 (2024), 2407.05743.

[70] S. Fleming, R. Hodges, and T. Mehen, Phys. Rev. D **104**, 116010 (2021), 2109.02188.

[71] M.-J. Yan and M. P. Valderrama, Phys. Rev. D **105**, 014007 (2022), 2108.04785.

[72] Z.-S. Jia, M.-J. Yan, Z.-H. Zhang, P.-P. Shi, G. Li, and F.-K. Guo, Phys. Rev. D **107**, 074029 (2023), 2211.02479.

[73] Z.-S. Jia, Z.-H. Zhang, G. Li, and F.-K. Guo, Phys. Rev. D **108**, 094038 (2023), 2307.11047.

[74] L. Dai, S. Fleming, R. Hodges, and T. Mehen, Phys. Rev. D **107**, 076001 (2023), 2301.11950.

[75] F.-Z. Peng, M.-J. Yan, and M. Pavon Valderrama, Phys. Rev. D **108**, 114001 (2023), 2304.13515.

[76] T. Ji, X.-K. Dong, F.-K. Guo, C. Hanhart, and U.-G. Meißner (2025), 2502.04458.

[77] F.-Z. Peng, M.-J. Yan, M. Sánchez, and M. Pavon Valderrama, Phys. Lett. B **846**, 138207 (2023), 2211.09154.

[78] M.-L. Du, V. Baru, F.-K. Guo, C. Hanhart, U.-G. Meißner, J. A. Oller, and Q. Wang, Phys. Rev. Lett. **124**, 072001 (2020), 1910.11846.

[79] C. Fernández-Ramírez, A. Pilloni, M. Albaladejo, A. Jackura, V. Mathieu, M. Mikhasenko, J. A. Silva-Castro, and A. P. Szczepaniak (JPAC), Phys. Rev. Lett. **123**, 092001 (2019), 1904.10021.

[80] Z.-G. Wang and X. Wang, Chin. Phys. C **44**, 103102 (2020), 1907.04582.

[81] M.-Z. Liu, Y.-W. Pan, F.-Z. Peng, M. Sánchez Sánchez, L.-S. Geng, A. Hosaka, and M. Pavon Valderrama, Phys. Rev. Lett. **122**, 242001 (2019), 1903.11560.

[82] B. Wang, L. Meng, and S.-L. Zhu, Phys. Rev. D **101**, 034018 (2020), 1912.12592.

[83] H.-X. Chen, W. Chen, X. Liu, and X.-H. Liu, Eur. Phys. J. C **81**, 409 (2021), 2011.01079.

[84] C. W. Xiao, J. J. Wu, and B. S. Zou, Phys. Rev. D **103**, 054016 (2021), 2102.02607.

[85] M.-J. Yan, F.-Z. Peng, M. Sánchez Sánchez, and M. Pavon Valderrama, Phys. Rev. D **107**, 074025 (2023), 2207.11144.

[86] S. X. Nakamura and J. J. Wu, Phys. Rev. D **108**, L011501 (2023), 2208.11995.

[87] J.-T. Zhu, S.-Y. Kong, and J. He, Phys. Rev. D **107**, 034029 (2023), 2211.06232.

[88] M.-J. Yan, F.-Z. Peng, and M. Pavon Valderrama, Phys. Rev. D **109**, 014023 (2024), 2304.14855.

[89] K.-S. Qiao and B.-S. Zou, Phys. Rev. D **111**, 056029 (2025), 2412.03216.

[90] A. Gal and H. Garcilazo, Phys. Rev. Lett. **111**, 172301 (2013), 1308.2112.

[91] A. Gal and H. Garcilazo, Nucl. Phys. A **928**, 73 (2014), 1402.3171.

[92] F. Etminan, H. Nemura, S. Aoki, T. Doi, T. Hatsuda, Y. Ikeda, T. Inoue, N. Ishii, K. Murano, and K. Sasaki (HAL QCD), Nucl. Phys. A **928**, 89 (2014), 1403.7284.

[93] T. Iritani et al. (HAL QCD), Phys. Lett. B **792**, 284 (2019), 1810.03416.

[94] T. Sekihara, Y. Kamiya, and T. Hyodo, Phys. Rev. C **98**, 015205 (2018), 1805.04024.

[95] M. Ablikim et al. (BESIII), Phys. Rev. D **87**, 032008 (2013), 1211.5668.

[96] V. A. Dorofeev et al., Eur. Phys. J. A **60**, 105 (2024), 2306.07779.

[97] S. Navas et al. (Particle Data Group), Phys. Rev. D **110**, 030001 (2024).

[98] T. Hatsuda, PoS **QCHSC24**, 002 (2025), 2507.08359.

Appendix: Two-pion and Kaon exchange in $N\phi$ scattering

In this appendix, we examine possible contributions from two-pion and kaon exchange to the $N\phi$ interaction. The corresponding Feynman diagrams are shown

in Fig. 9. Both S - and P -wave transitions are in principle allowed. The S -wave transition (denoted by the rectangle) is governed by the Weinberg-Tomozawa (WT) term at leading order in chiral perturbation theory, while the P -wave transition arises from the axial coupling.

However, the WT interactions for elastic $\phi\pi$, ϕK , and $\phi\bar{K}$ scattering vanish at leading order [33]. As a consequence, the contribution from the two-pion exchange diagram shown in Fig. 9(a) identically vanishes. This situation is in contrast to the case of two-pion exchange in $J/\psi N$ scattering, where a nonvanishing $J/\psi\pi \rightarrow J/\psi\pi$ transition exists, as illustrated in Fig. 1(c) of Ref. [32]. Similarly, the kaon-exchange contribution shown in Fig. 9(b) also vanishes at this order. This again differs from the mechanism in Fig. 1(d) of Ref. [32], where the corresponding meson-hadron transition is allowed. Therefore, neither two-pion nor kaon exchange generates a long-range interaction in $N\phi$ scattering in two-point loop. These support the conclusion drawn in the main text: the $N\phi$ interaction near threshold is not dominated by conventional one- or two-meson exchange mechanisms, but is instead driven by the promoted triangle diagram involving near-on-shell intermediate states.

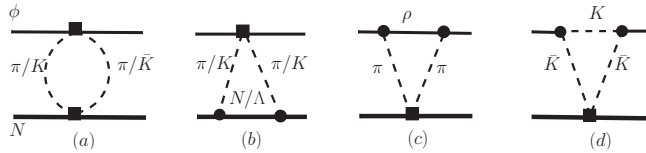


FIG. 9: The Feynman diagrams of $N\phi$ scattering with two-pion and Kaon exchange. The rectangle and the solid circle stand for the S - and P -wave transitions, respectively.

In Figs. 9(c) and (d), the ϕ meson couples to $\rho\pi$ and $K\bar{K}$, respectively. According to the PDG [97], the branching ratio of $\phi \rightarrow K\bar{K}$ is about 5.4 times larger than that of $\phi \rightarrow \rho\pi$, despite the fact that the available phase space for $\phi \rightarrow K\bar{K}$ is smaller than that for $\phi \rightarrow \rho\pi$. This feature indicates a much stronger effective coupling of the ϕ meson to the $K\bar{K}$ channel compared to the $\rho\pi$ channel.

In the baryon exchange in the triangle diagrams, the poles ($N(1440)$, Δ) in $N\pi$ scattering are known to be broad and located far away from the $N\pi$ threshold. As a consequence, the enhancement induced by $N\pi$ rescattering in $N\phi$ scattering is much weaker than that generated by $N\bar{K}$ rescattering promoted by the near-threshold $\Lambda(1405)$ pole. Meanwhile, the intermediate N and Λ in diagram (b) are away from their mass-shell. As a result, the N^3LO two-pion exchange in Ref. [98] is not kinematically and differs from the mechanism in the main text. Therefore, the contribution from the diagram in Fig. 9(c) is expected to be suppressed compared to that in Fig. 9(d).

Furthermore, there exists a clear separation of scales between the two mechanisms. The effective ranges associated with two-pion and two-kaon exchange are of order $1/(2m_\pi)$ and $1/(2m_K)$, respectively. When the kaons in Fig. 9(d) are nearly on shell, the typical momentum $\sqrt{m_K(m_\phi - 2m_K)}$ introduces a new dynamical scale in $N\phi$ scattering. We focus on interactions with a range of order $1/\sqrt{m_K(m_\phi - 2m_K)}$, for which the two-kaon exchange mechanism is expected to be particularly relevant compared with the two-pion exchange.